Synthesis, Structure Peculiarities and Acid−Basic Behaviour of Triazoleporphyrazines

Mikhail K. Islyaikin[a,@], Olga N. Trukhina[a], Yulia V. Romanenko[c], Elena A. Danilova[a], and Olga G. Khelevina[b]

[a]*Department of Fine Organic Synthesis, Ivanovo State University of Chemistry and Technology, Ivanovo, 153000, Russia*
[b]*Department of Organic Chemistry, Ivanovo State University of Chemistry and Technology, Ivanovo, 153000, Russia*
[c] *Department of Polymers, Ivanovo State University of Chemistry and Technology, Ivanovo, 153000, Russia*
[@]*Corresponding author E-mail: islyaikin@isuct.ru*

Recent advances in the chemistry of triazoleporphyrazines, structural analogues of porphyrazine containing one 1,2,4-triazole ring instead of one of pyrrole subunits, are reviewed. Experimental data of stepwise protonation equilibrium are discussed and basicity centers of macroheterocyclic compounds are revealed. Spacial configurations and electronic structure peculiarities of the tautomers of triazoleporphyrazine and its protonated forms are calculated using DFT method. Aromaticity of various conjugation contours is evaluated using HOMA and NICS criteria.

Introduction

Macroheterocyclic compounds (porphyrins, porphyrazines, phthalocyanines) having a high symmetry tetrapyrrole macrocycle as a basis of their structure are of an outstanding importance. Porphyrins,[1,2] porphyrazines[3] and phthalocyanines[4,5] are substances with numerous biological and practical applications. Many research efforts were focused also on noncentrosymmetric compounds.[6] The lack of a symmetry center in their molecules makes them good targets for development of materials with non-linear optical applications.[7] Amphiphilic structure of the molecules is especially appropriate for the Langmuir-Blodgett films formation. Besides, they can be used as constructional blocks for molecular ensembles of nanosized supramolecular architectures.[8,9]

There are two main approaches to reduce symmetry of these macrocycles. The first one is introduction of different substituents to the periphery of the macrocycle to form the noncenrosymmetric molecules.[10] The presence of substituents provokes perturbation of molecular orbitals and as consequence induces the permanent dipole moment. In this connection, significant attention has been paid to the synthesis of substituted phthalonitriles and their functional derivatives used as phthalocyanines precursors.[11-13] The second way to gain access to noncentrosymmetric macrocycles is a modification of a central core by formal substitution of one of pyrrole or isoindole rings by another cycle. Azoles seem to be the most attractive heterocycles for core modification since they are heteroanalogues of pyrrole. Using azoles as a heteroaromatic subunit, one can assemble ABBB-systems with 18 π-electrons containing inner cross similar to that of porphyrazines and phthalocyanines. Moreover, a possibility to influence deeply conjugation system *via* lone electron pairs of heteroatoms of azole subunits seems to be very attractive.

Following this strategy the noncentrosymmetric porphyrin[14] and phthalocyanine[6,15] analogues have been synthesized recently. The triazolephthalocyanines, structural analogues of phthalocyanine, have been extensively studied by the group of Prof. Torres.[16-19] In particular, it has been shown that these compounds have permanent dipole moments and, hence, ability to form well-ordered Langmuir-Blodgett monolayers[20] and to produce the second harmonic generation[21] as well.

Recently the first representatives of a new class of noncentrosymmetric tetrapyrrole macrocycles – triazoleporphyrazines, have been synthesized.[22] These compounds should be considered as analogues of porphyrazine in which one pyrrole subunit is replaced by 1,2,4-triazole.*

Synthesis of Substituted Triazoleporphyrazines

Hexa(4-*tert*-butylphenyl)triazoleporphyrazine (**1**) and its N-substituted analogue (**2**) was synthesized by condensation of 3,4-bis(4-*tert*-butylphenyl)-2,5-pyrrolinediimine and 3,5-diamino-1,2,4-triazole (guanazole) or 1-dodecyl-3,5-diamino-1,2,4-triazole in stoichiometric ratio (3:1), in anhydrous *n*-butanol at reflux (Scheme 1). High solubility of these products (**1**, **2**) in organic solvents allows to purify them by column chromatography on silica gel.

The metal complexes (**3-5**) were prepared[22] by treatment of metal free triazoleporphyrazine (**1**) with an appropriate metal acetate in DMF at 100 ºC in 78-90% yields (Scheme 2).

Alternatively, nickel (II) triazolephthalocyanine was synthesized by crossover macrocyclization of 3,4-bis(4-*tert*-butylphenyl)-2,5-pyrrolinediimine and guanazole in 2-ethoxyethanol at 135 ºC, in presence of a metal template. However, this method seems to be less efficient than the stepwise procedure. Thus, the complex **3** bearing one nickel (II) ion within its central binding core was obtained with 14% yield.

* Correspondingly they can be named more correctly as diazasubstituted porphyrazines, *i.e.* 2,3-diazaporphyrazines (Edr).

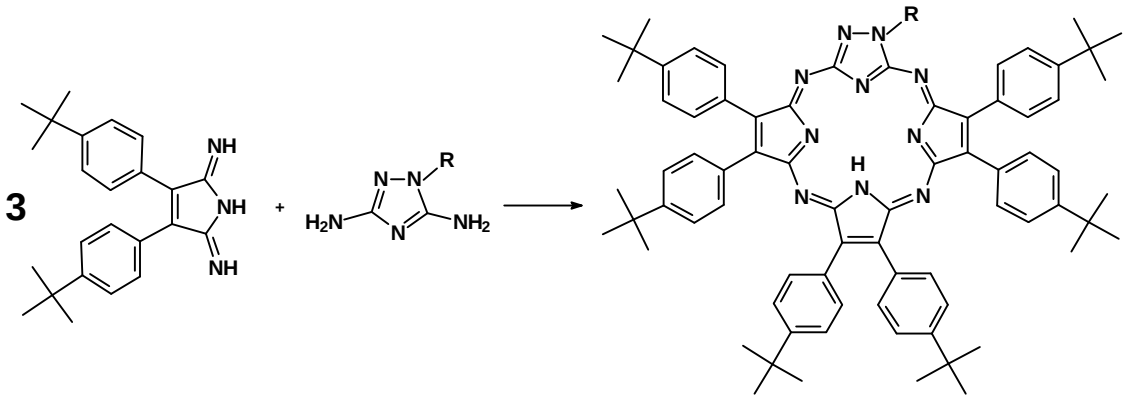

Scheme 1. Synthesis of substituted triazoleporphyrazines.

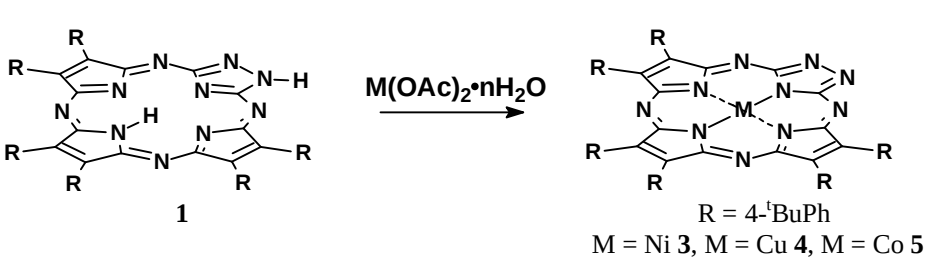

Scheme 2. Preparation of metal complexes of triazoleporphyrazine **1**.

Compounds (**1-5)** were characterized by elemental analysis, UV-vis, IR, NMR and MS data. The signals of the molecular ion [M] (*m/z* = 1108.6) and the monoprotonated form $[M+H]^+$ (*m/z* = 1109.5) were found in MALDI TOF spectra of **1**.

The absorption bands in the IR-region 3200–3500 cm^{-1} are of especial importance for determining the position of hydrogen atom in the triazole ring. One can see three bands at 3430, 3379, 3299 cm^{-1} in the spectrum of **1** (Figure 1a). The signal at 3299 cm^{-1} can be assigned to stretching vibrations of pyrrole N-H bond. Its position is low variable from the state of the compound on going from a solid state to a chloroform. Thus, the absorption band is slightly shifted up to 3302 cm^{-1} in the IR-spectrum of **1** in chloroform. Moreover, the band appears at 3299 cm^{-1} in the spectrum of **2** (Figure 1b) and disappears in the spectrum of the complex **3** (Figure 1c). The stretching vibrations of the triazole N-H bond result in the second band at 3379 cm^{-1} in the IR-spectrum of **1**. It is noted that this band is absent in spectra of the dodecyl-substituted compound **2** or the metal complexes (**3-5)**.

The proton absorption of *tert*-butyl-group is detected at 1.25 ppm in the ^{1}H NMR spectrum of **1** in $C_2D_2Cl_4$ solution. The low-pronounced multiplet at 7.26 ppm is assigned to protons of phenyl rings. The signal broadening at 15.24 ppm is a consequence of transannular protons absorption of the pyrrole N-atoms. The signal becomes well-pronounced and shifts to 15.14 ppm at 120 °C, whereas it becomes hardly observable at -30 °C. Absorption at low external magnetic field shows the absence of strong ring current within the core area of the macrocycle **1**. This provides evidence to weak conjugation in the molecules of **1.**

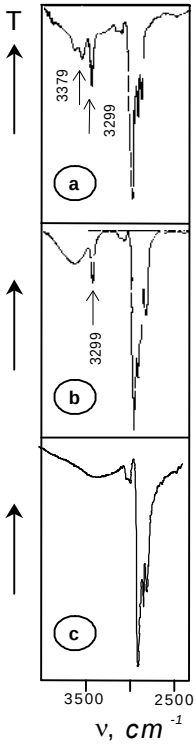

Figure1. IR spectra of triazoleporphyrazines a – **1**, b – **2**, c – **3**.

Structure Peculiarities

A molecule of triazoleporphyrazine **6** can be represented by three tautomers: **7a, 7b, 7c** (Scheme 3).

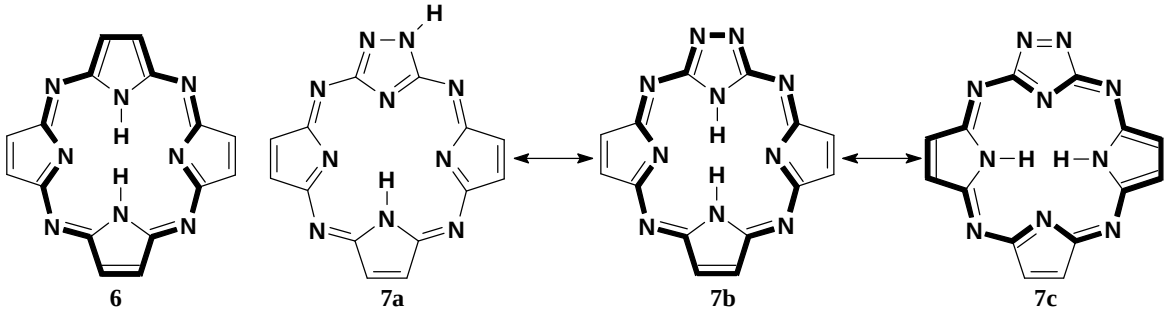

Scheme 3. Porphyrazine (**6**) and tautomerism of triazoleporphyrazines.

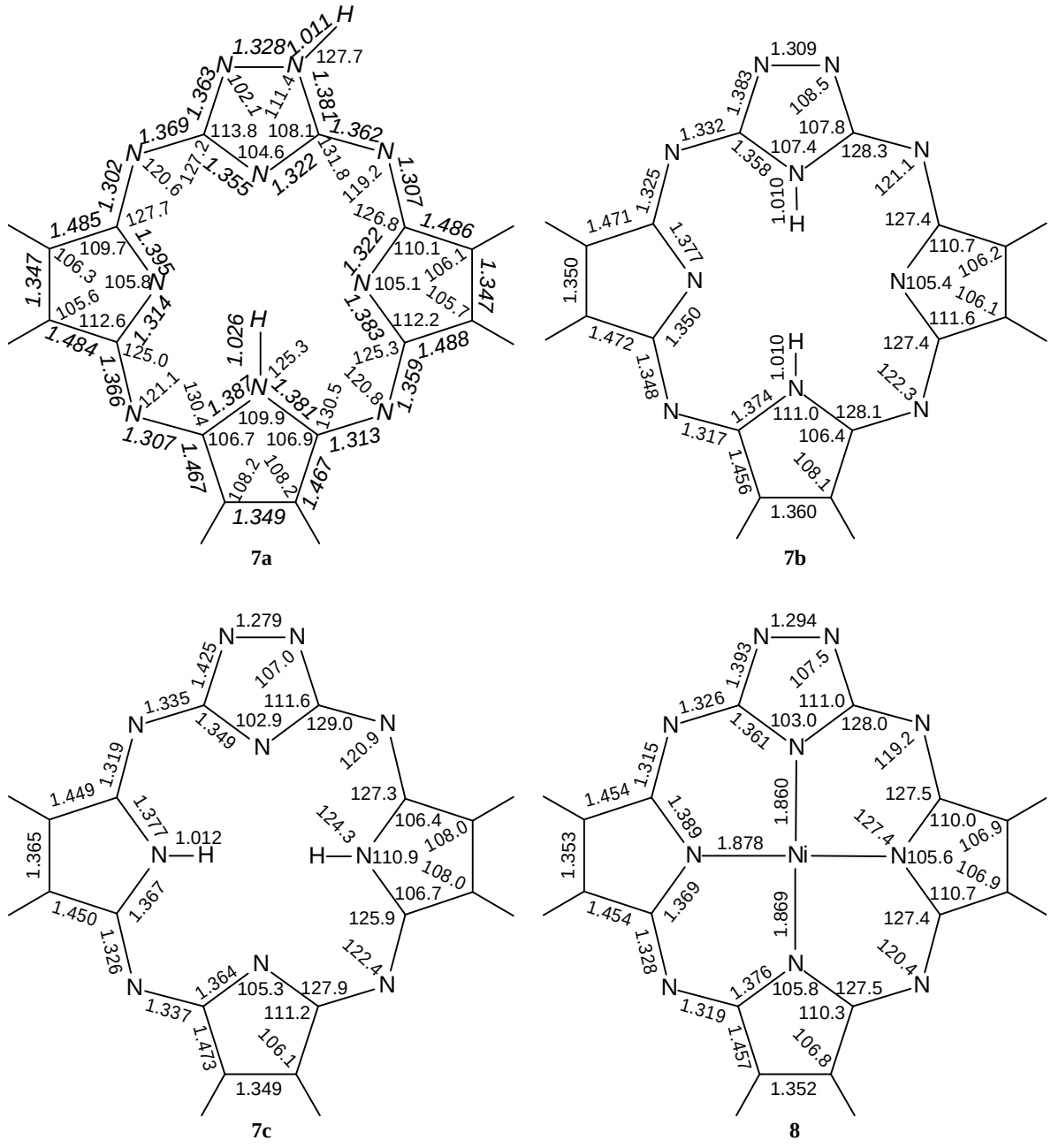

Figure 2. Bond lengths (Å) and bond angles (degrees) of **7a-c**, and **8** structures optimized at DFT B3LYP/6-31G (*d*, *p*) level.

Since the monocrystals appropriate for X-Ray study have not been available until now, the geometry and electron configuration of porphyrazine (**6**), the tautomers (**7a-c**) and the nickel complex (**8**) of triazoleporphyrazine were calculated using quantum chemistry methods. The full geometry optimization as well as the NBO and GIAO calculations were carried out at the DFT level. The functional employed was the Becke three parameter (B3LYP) hybrid functional at the 6-31G(*d*,*p*) basis set. The results are shown in Tables 1, 2 and Figures 2, 3.

Comparison of the calculated energies (Table 1) shows that **7c** is the most energy-advantageous compound among the tautomers **7a-c**. Besides, **7c** has the structure of the inner macrocycle most closely corresponding to that of porphyrazine.

Table 1. Total (*E*) and relative (ΔE) energies, ionization potentials (IP) and dipole moments (μ) of structures **6**, **7a-c** and **8** optimized at DFT B3LYP/6-31G(*d,p*) level.

Structure	*E*, a.u.	ΔE_{rel},[a] kJ·mol^{-1}	IP, eV	μ, D
6	-1053.72663826	-	5.82	0.00
7a	-1085.75771329	52.50	6.45	2.66
7b	-1085.77012851	19.89	6.48	7.21
7c	-1085.77770003	0.00	6.36	6.13
8	-2592.8681607	-	6.41	6.67

[a]For the structures **7a-c**.

It should be noted that N-N bond length of triazole ring decreases in the order **7a>7b>7c** and approaches N=N double bond in the molecule **7c** (Figure 2), whereas the length of the N–C bond linking the N–N group with the inner macrocycle increases in the sequence **7a>7b>7c** reaching 1.425 Å for **7c**. This fact indicates that an interaction between N–N fragment and the rest of the system becomes weaker in this series. Thus, the structure **8** has the length of the N-N bond equal to 1.294 Å which is between those of **7b** and **7c** due to substitution of both inner hydrogen atoms of the macrocycle for the metal atom.

Molecule of triazoleporphyrazine (**7**) as well as molecule of porphyrazine (**6**) are systems with multicontour conjugation. It was attractive to estimate the effect of tautomerism on aromaticity. Thus, total aromaticity of the macrocycle molecules and local aromaticity of various conjugation contours were evaluated using Harmonic Oscillator Model of Aromaticity (HOMA)[23,24] and Nucleus Independent Chemical Shifts (NICS)[25] criteria.

HOMA and NICS criteria were obtained[26] on the basis of geometries shown in Figure 2. Table 2 displays the values calculated for HOMA and its components EN and GEO, and NICS indices of the compounds of interest. It is obvious that the aromaticity of triazoleporphyrazine is affected by tautomerism arising from the hydrogen atoms migration.

Following the HOMA criteria calculated for the whole molecules (Table 2), the aromaticity increases in the sequence **7a<7b<7c<8,** which is in a good agreement with equalization of the bonds lengths.

The increase of total aromaticity in the **7a<7b<7c** order along with the decrease of local triazole aromaticity is observed. This fact confirms the idea that the triazole ring which is involved into a macrocyclic conjugation system should lose a part of its aromaticity. Interaction of triazole ring with conjugation system of the inner macrocycle results in the N-N bond isolation and enlarged alternation of double/single bonds of the triazole ring. The GEO indices

Table 2. EN, GEO и HOMA indices for **7a-c** and **8** structures optimized at DFT B3LYP/6-31G (d, p) level[a].

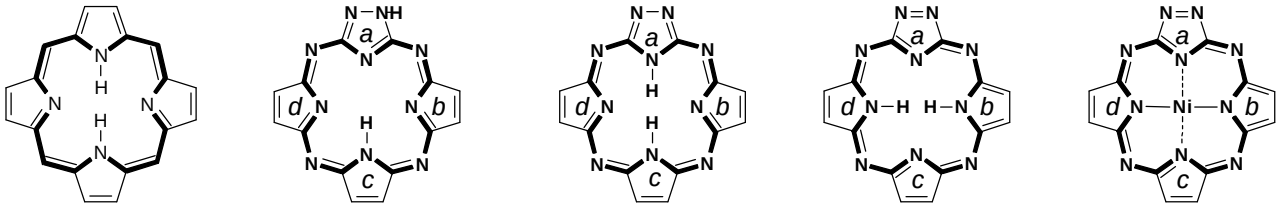

6 **7a** **7b** **7c** **8**

Structure	EN	GEO	HOMA
Porphyrazine **6**	0.115	0.322	0.562
internal cross	0.022	0.036	0.942
7a (whole system)	0.122	0.464	0.414
triazole ring *a*	0.044	0.034	0.922
internal cross	0.015	0.094	0.892
7b (whole system)	0.103	0.322	0.567
triazole ring *a*	0.081	0.032	0.887
internal cross	0.018	0.039	0.943
7c (whole system)	0.098	0.287	0.615
triazole ring *a*	0.118	0.225	0.657
internal cross	0.016	0.036	0.948
8 (whole system)	0.080	0.277	0.643
triazole ring *a*	0.090	0.074	0.835
internal cross	0.019	0.069	0.913

[a]The EN, GEO, HOMA indices calculated for the free base porphyrin are 0.107, 0.240 and 0.666 respectively.

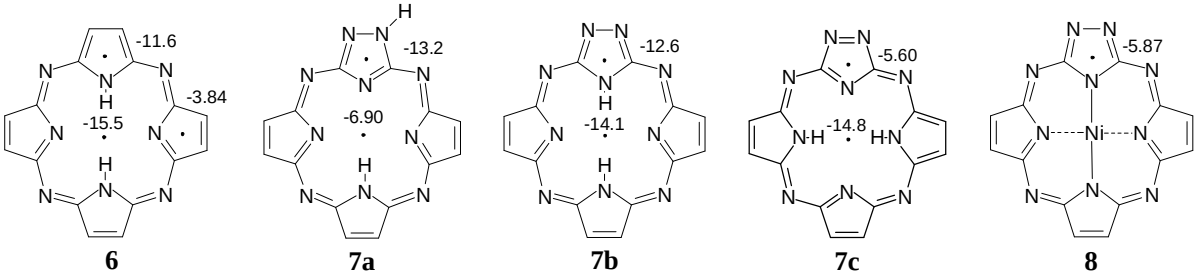

6 **7a** **7b** **7c** **8**

Figure 3. Calculated NICS values (ppm) of the studied compounds.

increase from 0.034 to 0.225 for **7a-c (**Table 2). The inner macrocycle aromaticity increases from **7a** (HOMA=0.892) to **7c** (HOMA=0.948).

The NICS magnetic criteria confirm the tendency of aromaticity changes revealed by the HOMA criterion in the consecution **6**, **7a-c**, **8** (Figure 3). They are based on the magnetic properties of π-electron systems and indicate that the compound **7a** has the lowest aromaticity (NICS=-6.90 ppm), whereas the compound **7c** is the most aromatic of tautomers (NICS=-14.80 ppm).

It was found that an internal cross ([16]heteroannulene contour) bearing 18 π electrons was the most aromatic part of the molecules.

UV-vis Characterisation

The UV-vis spectrum of the compound **1** (Figure 4) is formed of four strong absorption bands. The electron transfers within phenyl rings result in the strongest band at 244 nm. The band at 324 nm is the Soret band similar to the equivalent absorption of its porphyrazine counterpart.

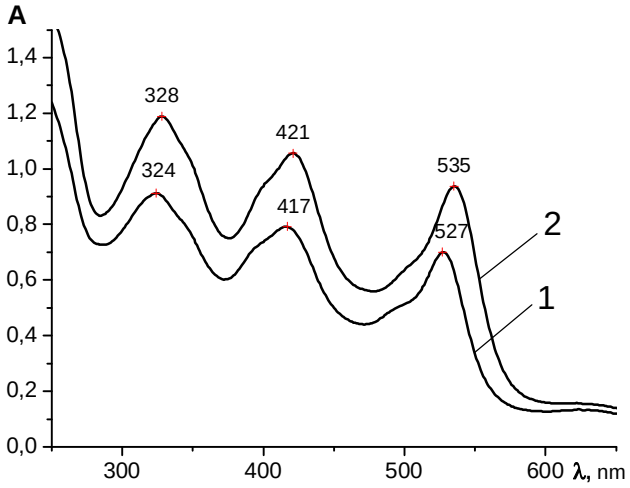

Figure 4. UV-vis spectra: 1 – **1**, $CHCl_3$, c=2.16·10^{-5} M; 2 – **2**, $CHCl_3$, c=1.71·10^{-5} M.

The strong band at 417 nm (or less intense band, red-shifted to 450 nm, in the spectrum of substituted porphyrazine) is a consequence of symmetry lowering due to the substitution of pyrrole fragment for triazole fragment in the molecular core.

The long-wave absorption band at 527 nm of substituted triazoleporphyrazine is hypsochromically shifted by 139 nm as compared with corresponding porphyrazine.[27] Thus, there is no effective conjugation in the macrocycle due to the presence of the triazole ring.

The peculiarities mentioned above are confirmed for the dodecyl-substituted compound **2**. Compounds **1** and **2** have the analogous spectral curves, that is a proof of similarity of their chromophoric systems. The presence of dodecyl substituent in **2** fixes the 1H form of the triazole ring. This fact shows the presence of hydrogen atom in position 1 within a triazole ring in triazoleporphyrazines **1** and **2**.[28] The absorption bands of **2** are slightly shifted hypsochromically due to weak +*I*-effect of dodecyl group.

The UV-vis spectra of the complexes **3-5** (Figure 5) have three regions: i) the long-wavelength absorption bands at 602-629 nm and the line broaderning at 570 nm (inflexion for **3** and **4**), ii) the broad band in the middle part of the spectrum at 472-518 nm, iii) two bands in UV region at 325-391 nm. The positions and intensities of the long-wave absorption bands argue for aromatic character of the metal complexes. Nature of the metal has an influence upon the position of the absorption bands. Bathochromic shift of the long-wavelength absorption band increases in the sequence Ni<Co<Cu.

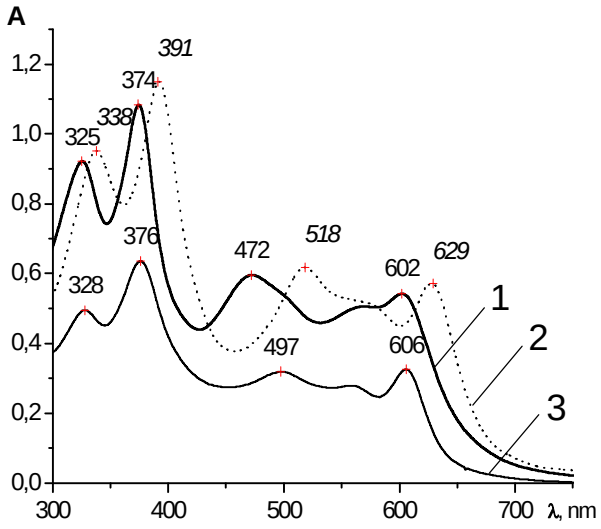

Figure 5. UV-vis spectra: 1 - M = Ni, 3, CH_2Cl_2,c=1.71·10^{-5} M; 2 - M = Cu, 4, $CHCl_3$, c=2.05·10^{-5} M; 3 - M = Co, 5, $CHCl_3$, c=1.03·10^{-5} M.

To clarify the nature of the absorption bands we carried out calculations of electron absorption spectra of the model molecules **7a-c** and **8** using ZINDOS method, their geometries were obtained using DFT B3LYP 6-31G(*d*,*p*) method. Essential results of our calculations are given in Table 3.

Table 3. Calculated values of energy of three high occupied molecular orbitals and three lower unoccupied molecular orbitals, energies of first singlet-singlet passages (Δ*E*) of **6, 7a-c, and 8** structures.

№	Energy of molecular orbital, eV						Δ*E*, eV
	LUMO+2	LUMO+1	**LUMO**	**HOMO**	HOMO-1	HOMO-2	
6	-0.33	-1.78	**-2.14**	**-6.22**	-8.63	-9.15	4.08
7a	-0.72	-1.29	**-2.40**	**-7.49**	-8.75	-9.32	5.09
7b	-0.85	-1.89	**-2.71**	**-6.91**	-9.13	-9.56	4.20
7c	-0.85	-2.28	**-2.42**	**-6.63**	-8.92	-9.70	4.21
8	-0.94	-2.11	**-2.64**	**-6.89**	-9.08	-9.14	4.25

It can be seen that substitution of one pyrrole subunit by 1,3,4-triazole moiety in porphyrazine core gives rise to stabilization of the highest occupied molecular orbitals (HOMO) and the lower unoccupied molecular orbitals (LUMO). However, occupied molecular orbitals are stabilized greater than virtual ones. This results in increasing of the energy gap between frontier orbitals of triazoleporphyrazine **7** in comparison with those of porphyrazine **6**. The difference between HOMO and LUMO positions becomes more pronounced in the sequence of the tautomers **7a-c**.

Acid–Base Behavior in Proton-Donating Media

In comparison with porphyrazine, triazole-porphyrazine has two extra nitrogen atoms (nitrogens of triazole ring), which could be considered as additional centers of protonation. Thus, sequential equilibria of protonation may be formulated as follows:

$MPz + H^+ \leftrightarrow MPzH^+$

$MPzH^+ + H^+ \leftrightarrow MPzH_2^{2+}$

and so on, where $MPzH^+$ and $MPzH_2^{2+}$ are the first and the second protonated forms of the MPz initial base, respectively.

The proton transfer from acid HA to base B is a complex process with the stages of the acid associate, H-associate, ion-ion associate and ionized protonated form. Formation of the first acid form of the compounds **1**, **2** and **4** is completed in media having acidities that are stronger than those of pure acetic acid, *i.e.* in H_2SO_4 – antipyrine – HOAc mixtures (H_0=3.95 for **1** and **2** and 4.60 for **4**). The *Q*-bands are shifted hypsochromically by 473, 376 and 755 cm^{-1}. The character of the spectral changes observed for **1** and **4** are shown in Figures 6 and 7**,** respectively. Taking into account that the shift of the *Q*-band maxima are observed in media with poor ionizing ability, it can be concluded that ion–ion associate is formed.

The logI_i–H_0 dependences are linear for **1**, **2** and **4** in benzene–acetic acid media (Figure 8). The slopes of the logI_i–H_0 lines are 0.97, 0.79 and 1.14 for **1**, **2** and **4**, respectively.

This result indicates that only one donor center is protonated by acid in all studied systems. Further increase of acidity leads to the rapid destruction of triazoleporphyrazines.

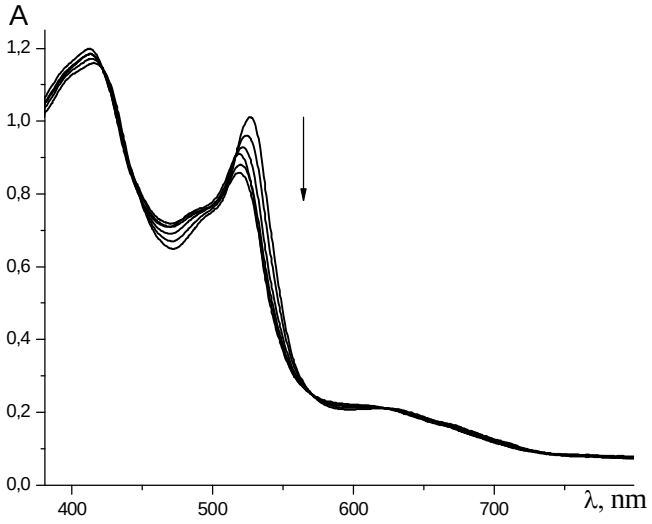

Figure 6. Changes of UV-vis spectrum of **1** in benzene-AcOH; H_0 decreases from 6.33 to 4.60.

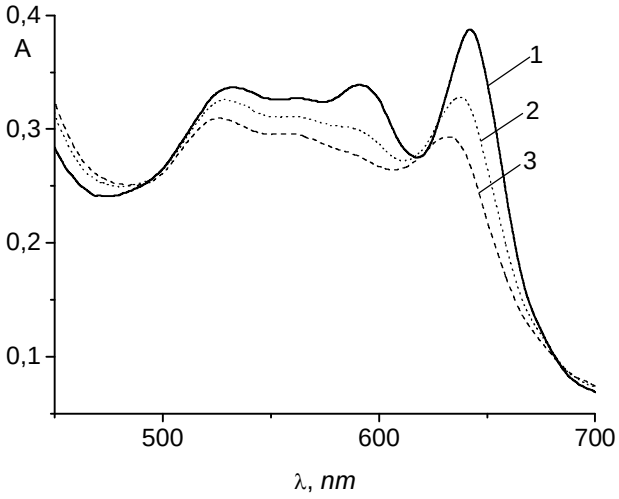

Figure 7. UV-vis spectra of solutions of **4** in (1) benzene, (2) benzene-HOAc (H_0=6.44), (3) benzene-HOAc (H_0=6.17).

To determine a position of protonation, the quantum chemistry calculations were carried out for modelling species: triazoleporphyrazine, 1-methyltriazoleporphyrazine, Zn-triazoleporphyrazine cores and their protonated forms.

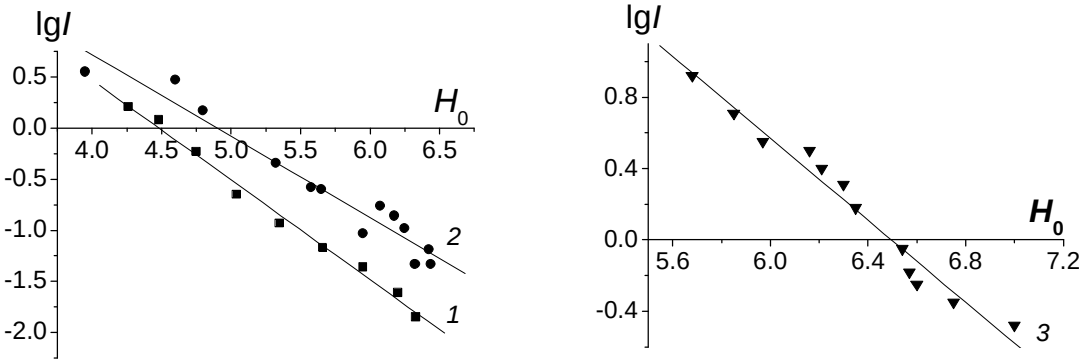

Figure 8. Relationships log*I*-H_0 for the equilibrium of the ion-ion associate formation in the benzene-acetic acid system. Series *1, 2, 3* correspond to compounds **1, 2, 4.**

Table 4. Heats of formation (ΔH_f), relative energies ($\Delta\Delta H_f$), ionization potentials (IP), dipole moments (μ), nitrogen atoms charges, and first singlet-singlet transitions (λ_{max}) of triazoleporphyrazine **7a** and its monoprotonated forms.

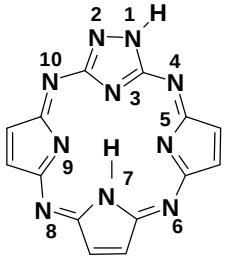

Proto-nated N-atom	ΔH_f, kcal mol^{-1}	$\Delta\Delta H_f$, kcal mol^{-1}	IP, e*V*	μ, *D*	charges on the nitrogen atoms, charge unit										λ_{max}* nm
					1	2	3	4	5	6	7	8	9	10	
-	350.01	-	9.11	3.07	-0.175	-0.025	-0.110	-0.086	-0.190	-0.146	-0.285	-0.100	-0.159	-0.012	478
1	522.42	33.69	12.65	4.46	-0.033	-0.136	-0.107	-0.168	-0.310	-0.172	-0.313	-0.130	-0.247	-0.094	279
2	506.79	18.06	12.64	4.38	-0.171	-0.151	-0.149	-0.141	-0.271	-0.153	-0.316	-0.154	-0.271	-0.142	273
3	488.73	0.00	12.89	2.37	-0.122	0.031	-0.212	-0.127	-0.361	-0.170	-0.321	-0.122	-0.307	-0.039	341
4	502.22	13.49	12.50	7.35	-0.194	0.028	-0.107	-0.184	-0.294	-0.144	-0.205	-0.017	-0.159	0.024	565
5	490.10	1.37	12.66	6.63	-0.136	0.026	-0.178	-0.037	-0.311	-0.216	-0.291	-0.027	-0.187	0.022	572
6	501.20	12.47	12.40	10.95	-0.150	0.020	-0.105	-0.014	-0.190	-0.189	-0.210	-0.014	-0.160	0.030	674
7	511.21	22.48	12.56	6.67	-0.135	0.038	-0.137	-0.015	-0.179	-0.018	-0.059	-0.010	-0.192	0.037	636

Found for the configurations optimized by AM1 method, UV-vis data calculated by ZINDOS, CI = 5*3.

Table 5. Heats of formation (ΔH_f), relative energies ($\Delta\Delta H_f$), ionization potentials (IP), dipole moments (μ), nitrogen atoms charges, and first singlet-singlet transitions (λ_{max}) of 1-methyltriazoleporphyrazine and its monoprotonated forms

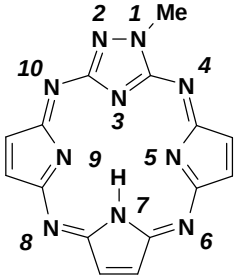

Proto-nated N-atom	ΔH_f, kcal mol^{-1}	$\Delta\Delta H_f$, kcal mol^{-1}	IP, e*V*	μ, *D*	charges on the nitrogen atoms, charge unit .										λ_{max}* nm
					1	2	3	4	5	6	7	8	9	10	
-	355.50	-	9.05	2.99	-0.131	-0.022	-0.110	-0.084	-0.186	-0.144	-0.284	-0.100	-0.158	-0.012	498
1	526.37	34.78	12.57	4.75	0.002	-0.130	-0.105	-0.164	-0.305	-0.171	-0.314	-0.129	-0.247	-0.089	276
2	508.83	17.24	12.52	5.19	-0.132	-0.147	-0.143	-0.139	-0.263	-0.151	-0.315	-0.151	-0.265	-0.135	276
3	491.59	0.00	12.79	2.71	-0.071	0.027	-0.209	-0.122	-0.353	-0.167	-0.321	-0.122	-0.304	-0.039	351
4	506.12	14.53	12.38	7.43	-0.149	0.029	-0.108	-0.180	-0.293	-0.146	-0.205	-0.018	-0.159	0.023	590
5	493.92	2.33	12.42	6.65	-0.086	0.024	-0.180	-0.036	-0.308	-0.218	-0.292	-0.029	-0.186	0.021	593
6	504.36	12.77	12.06	10.95	-0.103	0.019	-0.104	-0.014	-0.187	-0.188	-0.209	-0.014	-0.159	0.030	696
7	505.04	23.45	12.22	6.27	-0.075	0.043	-0.134	-0.009	-0.175	-0.017	-0.057	-0.010	-0.189	0.038	658

Found for the configurations optimized by AM1 method, UV-vis data calculated by ZINDOS, CI = 5*3.

Full geometry optimisation of these models was carried out by AM1 method. The optimized geometries were used to calculate the theoretical UV-vis spectra by ZINDOS method with configuration interactions. The results of the calculations are shown in the Tables 4-6.

Results of theoretical study show that most probably monoprotonation involves the internal nitrogen atom of the triazole ring of triazoleporphyrazines. The energy of long-wave singlet-singlet transitions increases in going from non-protonated to protonated forms, that corresponds to red shift of *Q*-bands. Theoretical studies agree with the experimental data for **1** and **2**. It's worthy to note that protonation of the isolated 1,2,4-triazole ring occurs on the nitrogen atom located at the position 4 of the ring.

Table 6. Heats of formation (ΔH_f), relative energies ($\Delta\Delta H_f$), ionization potentials (IP), dipole moments (μ), nitrogen atoms charges, and first singlet-singlet electron transitions (λ_{max}) of Zn-triazoleporphyrazine and its monoprotonated forms.

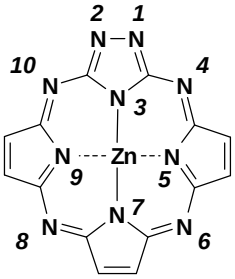

Proto-nated N-atom	ΔH_f, kcal mol^{-1}	$\Delta\Delta H_f$, kcal mol^{-1}	IP, e*V*	μ, D	charges on the nitrogen atoms, charge unit .										λ_{max}* nm
					1	2	3	4	5	6	7	8	9	10	
-	366.54	-	8.69	5.16	0.025	0.020	-0.306	-0.033	-0.324	-0.168	-0.318	-0.071	-0.308	-0.115	642
1	512.75	0.00	12.81	2.33	0.032	-0.119	-0.269	-0.022	-0.329	-0.160	-0.396	-0.185	-0.365	-0.097	374
3	529.03	16.28	12.81	4.40	0.082	0.082	-0.255	0.010	-0.330	-0.142	-0.402	-0.142	-0.330	0.010	629
4	514.19	1.44	12.37	4.62	0.019	0.081	-0.244	-0.137	-0.262	-0.047	-0.351	-0.157	-0.373	-0.029	665
5	524.97	12.22	12.73	5.38	0.078	0.060	-0.313	0.009	-0.236	-0.034	-0.323	-0.134	-0.400	-0.098	642
6	516.21	3.46	12.32	10.69	0.070	0.059	-0.355	-0.009	-0.261	-0.167	-0.265	-0.046	-0.347	-0.111	673
7	525.21	12.46	12.76	6.41	0.072	0.072	-0.399	-0.092	-0.318	-0.033	-0.234	-0.033	-0.319	-0.093	622

Found for the configurations optimized by AM1 method, UV-vis data calculated by ZINDOS, CI = 5*3.

In the metal complex, only *meso*-nitrogen atom can be protonated due to involvment of φ_n orbitals of the internal nitrogen atoms in the formation of donor-acceptor bonds with metal. The analysis of the heats of formation of the protonated forms shows that the structure with proton located at nitrogen atom N1 of triazole ring is more preferable.

The stability constants of the first acid forms pK_{s1} for **1**, **2** and **4** determined from Hammett's equation are 4.48 ± 0.18, 4.90 ± 0.32 and 6.50 ± 0.41, respectively.

The pK_{s1} values of **1** and **2** are of the same order of magnitude, suggesting that the protonation center is the same for both cases. Nevertheless, the basicity of **2** is significantly higher than that of **1**. To explain this fact one should consider the electron-donating (+I) effect of the alkyl substituent in the triazole ring containing the proton acceptor center. Introduction of the Cu^{2+} ion into the macrocycle (**4**) increases basicity by two orders of magnitude with respect to **1** and **2**.

This may indicate that the protonation center in the metal complex differs from that in **1** and **2**. In fact the protonation of the N atom located in position 4 of the triazole ring is impossible due to the presence of the metal cation at the center of the macrocycle cavity. Comparison of the pK_{s1} values obtained in this work for the triazoleporphyrazines (which ranged from 4.48 to 6.50) and those reported for the tetraazaporphyrins (1.00 and -1.33 for the octaphenyltetraazaporphyrin and its Cu complex, respectively) shows that the basicity increases when one pyrrole ring in the macrocycle is substituted by the triazole ring. It was shown previously that the first stage of the acid–base interaction in tetraazaporphyrins proceeds on one of the four *meso*-nitrogen atoms and leads to a bathochromic shift of the *Q*-band in the spectra.

To discover the possible effects of protonation on the molecular electronic structure of the triazoleporphyrazine at an adequate theoretical level with reasonably small computational effort, we selected three model protonated structures derived from the low-aromatic free-base triazoleporphyrazine **7a**. Two of these structures are protonated in the triazole ring, **9a** (position 4) and **9b** (position 3), and one is protonated in a *meso* N-atom, **9c** (Figure 9).

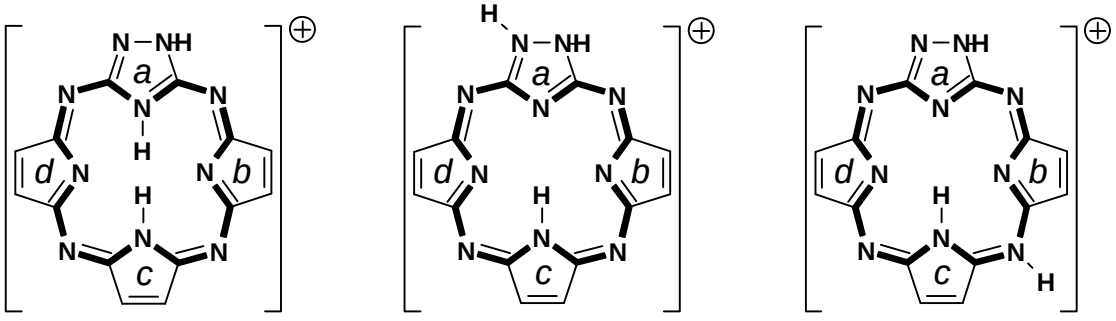

9a **9b** **9c**

Figure 9. Protonated (**9a–c**) structures of the unsubstituted free-base triazoleporphyrazine considered in this work. The internal cross of the structures is emphasized in bold.

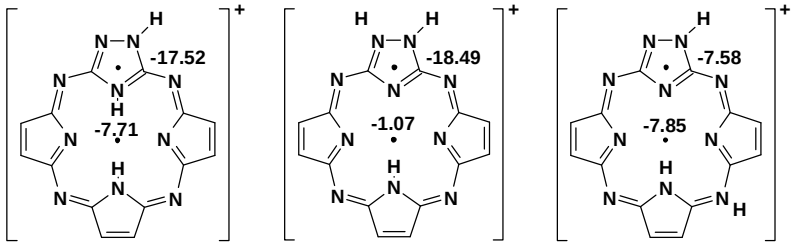

9a **9b** **9c**

Figure 10. Calculated NICS values (ppm) for the compounds **9a–c**.

The full geometry optimization performed at the DFT B3LYP/6–31(*d,p*) level yields plane configurations for the protonated forms **9a-c**. Upon protonation the planarity of the macrocycle is maintained, but its other geometric parameters are strongly changed. Considerable increases of the C–N (N–N) bond lengths are observed when the N atom captures a proton. For example, if a proton addition occurs to the nitrogen atom located at the position 4 of the triazole ring, the C–NH^+–C bonds elongate by more than 0.020Å. The magnitudes of total and relative electronic energies of the protonated forms **9a–c** are shown in Table 7.

Table 7. Total and relative energies of the protonated forms **9a-c**.

Structure	E_{tot}, au	ΔE_{rel}, au	ΔE_{rel}, kJ· mol^{-1}
9a	-1086.1604513	0.0000000	0
9b	-1086.1296643	0.0307870	80.75
9c	-1086.1359859	0.0244654	64.16

The cationic configuration **9a** bearing one proton at the position 4 of the triazole ring is found to be the most stable among the forms examined. Analysis of the charge distribution over all the molecule shows that in the cases of **9a** and **9b**, the positive charge is locally accumulated in the triazole ring, reaching values of +1.025 and +0.969, respectively. In contrast, the positive charge is more uniformly distributed over the whole molecule when the proton addition takes place along the exocyclic *meso* atom.

In order to estimate possible influence of the protonation on the aromatic properties, both geometry (EN, GEO and HOMA) and magnetic (NICS) based criteria of aromaticity were evaluated for the protonated forms of triazoleporphyrazine.

Table 8 gives the calculated values of geometry-based criteria of aromaticity for the systems under investigation.

In contrast to **9b**, proton addition to either the position 4 of the triazole ring (structure **9a**) or to the exocyclic-*meso*-N atom (structure **9c**) leads to equalization of the bond lengths in the cations. The GEO values decrease to 0.450 and 0.407 in **9a** and **9c**, respectively. The average bond lengths of these cations tend towards the optimal magnitude (EN criterion).

In **9a**, the formation of a porphyrazine-like internal cross explains the global increase in the HOMA, but simultaneously the local HOMA aromaticity index of triazole ring increases up to 0.956.

The description of the aromaticity based on geometry criteria is in a good agreement with that obtained by means of magnetic-based criteria (NICS).

Table 8. EN, GEO and HOMA indices for protonated forms **9a–c** optimized by B3LYP/6–31G(d,p).

Structure	EN	GEO	HOMA
9a (whole system)	**0.117**	**0.450**	**0.433**
Triazole ring (a)	0.028	0.016	0.956
Pyrrole ring (b)	0.346	0.767	-0.113
Pyrrole ring (c)	0.322	0.506	0.172
Pyrrole ring (d)	0.344	0.732	-0.076
Internal cross	0.019	0.077	*0.904*
9b(whole system)	**0.133**	**0.541**	**0.326**
Triazole ring (a)	0.057	0.037	0.906
Pyrrole ring (b)	0.371	0.959	-0.330
Pyrrole ring (c)	0.357	0.566	0.077
Pyrrole ring (d)	0.371	0.959	-0.330
Internal cross	*0.011*	*0.078*	*0.911*
9c (whole system)	**0.111**	**0.407**	**0.482**
Triazole ring (a)	0.040	0.053	0.907
Pyrrole ring (b)	0.264	0.715	0.021
Pyrrole ring (c)	0.256	0.391	0.353
Pyrrole ring (d)	0.402	0.666	-0.068
Internal cross	*0.018*	*0.124*	*0.858*

The value of the NICS index calculated for the center of the macrocycle **9a** (Figure 10) changes from -6.90 (neutral molecule) to -7.71 ppm, *i.e.* the aromaticity increases. Similar behavior was observed for the triazole ring of **9a**: the proton addition to the position 4 of the triazole ring (**9a**) produces an increase of the local aromaticity of this group. The NICS value of the center of the triazole ring changes from -13.20 (neutral molecule) to -17.52 (**9a**) ppm. This aromaticity increase for the structure **9a** can also serve as an explanation of the hypsochromic displacement of the absorbtion band.

Strong alternation of double and single bonds of the pyrrole rings *b* and *d* induces a considerable increase of the GEO values (Table 8) calculated for the structure **9b**. Therefore, global aromaticity of the ion decreases as the value obtained for the global HOMA (0.326) indicates.

The NICS value calculated for the center of the **9b** macrocycle cavity (-1.07 ppm) confirms very low aromatic character of this cation. The most aromatic part of this cation is the internal cross (depicted in Figure 9 in bold) as the HOMA index 0.911 obtained for this part of the molecule (Table 8) indicates. Accordingly, the single protonation of the triazoleporphyrazine throughout the position 4 of the triazole ring acts as an intramolecular switch for aromaticity.

In the case of exocyclic N atom (**9c**) protonation the HOMA increases up to 0.482. This increase is caused mostly by the HOMA contributions of pyrrole rings to the HOMA of the whole system. Since the N_{meso}-C bond lengths become elongated, the HOMA value of the internal cross decreases from 0.891 (neutral molecule) to 0.858 (**9c**). However, the N atom which is the acceptor of a proton is maintained as sufficiently good conductor of electron effects over molecule **9c**, as the NICS value of -7.85 ppm indicates.

Conclusion

Behaviour of hexakis(4-*tert*-butylphenyl)triazole-porphyrazine, its Cu complex and its 1-dodecyl derivative in proton-donating media was investigated. It was found that triazoleporphyrazines can be protonated in a proton-donating medium with poor ionizing ability (HOAc–benzene) forming ion–ion associates. Stability constants of the acid forms show that replacement of pyrrole moiety in porphyrazine by triazole ring increases basicity. Protonation of the triazoleporphyrazines results in a hypsochromic shift of the *Q*-bands in their UV–visible spectra.

Quantum chemical calculations show that the protonation of the triazoleporphyrazines strongly influences both their molecular electron structure and aromaticity. Investigations of the protonated forms confirm that the high basicity of triazoleporphyrazines is conditioned by protonation of the nitrogen atom located at the position 4 of the triazole ring, the corresponding protonated form has more aromatic character than the neutral structure. However, addition of one proton to the nitrogen atom at the position 4 of the triazole ring is responsible for the dramatic macrocycle aromaticity decrease. Hence one may consider the triazoleporphyrazines as an intramolecular switch for aromaticity.

References

1. Berezin B.D. *Koordinazionnye soedinenija porfirinow i ftalotcianinow.* [*Coordination compounds of porphyrines and phthalocyanines*] Moskwa, Nauka **1978**, 280. (in Russ.)
2. *The Porphyrin Handbook* Vols. 1-10 (Kadish K.M, Smith K.M, Guilard R., Eds) San Diego, Academic Press, **2000**.
3. Stuzhin P.A, Ercolani C. Porphyrazines with Annulated Heterocycles, in *The Porphyrin Handbook* (Kadish K.M., Smith K.M., Guilard R., Eds) Ch. 101, Amsterdam, Academic Press, **2003**, *15*, 263-364.
4. Leznoff C.C. In *Phthalocyanines: Properties and Applications* Vols. 1-4 (Leznoff C.C., Lever A.B.P., Eds), New York, VCH, **1989-1996**.
5. *The Porphyrin Handbook* Vols. 15–20 (Eds. Kadish K.M., Smith K.M., Guilard R.) Amsterdam, Academic Press, **2003**.
6. Rodríguez-Morgade M.S., De la Torre G., Torres T. Design and Synthesis of Low-Symmetry Phthalocyanines and Related Systems, in *The Porphyrin Handbook* Ch. 99 (Kadish K.M., Smith K.M., Guilard R., Eds), Amsterdam, Academic Press, **2003**, *15*, 125 – 160.
7. De la Torre G., Vazquez P., Agullo-Lopez F., Torres T.J. *Chem. Rev*. **2004**, *10*, 3723-3750.
8. De la Torre G., Blau W., Torres T.J. *Nanotechnology* **2003**, *14*, 765–771.
9. Guldi D.M., Gouloumis A., Vazquez P., Torres T., Georgakilas V., Prato M. *J. Am. Chem. Soc*. **2005**, *127*, 5811-5813.
10. Böhme R., Breitmaier E. J. *Synthesis* **1999**, *12*, 2096–2102.
11. Sharman W.M., Van Lier J.E. Synthesis of Phthalocyanine Precursors, in *The Porphyrin Handbook* (Kadish K.M., Smith K.M., Guilard R., Eds) Ch. 97, Amsterdam, Academic Press, **2003**, *15*, 1–60.
12. Leznoff C.C., Terekhov D.S., McArthur C.R., Vigh S., Li J. *Can. J. Chem.* **1995**, *73*, 435-443.
13. Wang J., Khanamiryan A.K., Leznoff C.C. *J. Porphyrins Phthalocyanines* **2004**, *8*, 1293-1299.
14. Latos-Grażyński L. Core-Modified Heteroanalogues of Porphyrins and Metalloporphyrins, in *The Porphyrin Handbook* (Kadish K.M., Smith K.M., Guilard R., Eds.) Ch. 14. Amsterdam, Academic Press, **2003**, *2*, 61-416.
15. Kudrik E.V., Islyaikin M.K., Smirnov R.P. *Zh. Org. Khim.* **1997**, *33*, 1107-1110. (Russ).
16. Fernández-Lázaro F., Sastre A., Torres T. *J. Chem. Soc., Chem. Com.* **1994**, 1525-1526.
17. Nicolau M., Cabezón B., Torres T. *J. Org. Chem.* **2001**, *66*, 89–93.
18. Esperanza S., Nicolau M., Torres T. *J. Org. Chem*. **2002**, *67*, 1392-1395.
19. Nicolau M., Cabezón B., Torres T. *Coord. Chem. Rev*. **1999**, *190-192***,** 231-243.
20. Armand F., Martínez-Díaz M.V., Cabezón B., Albouy P.-A., Ruaudel-Teixier A., Torres T. *J. Chem. Soc., Chem. Commun.* **1995**, 1673-1674.
21. Rojo G., Agulló-López F., Cabezón B., Torres T., Brasselet S., Ledoux I., Zyss J. *J. Phys. Chem., B* **2000**, *104*, 4295-4299.
22. Islyaikin M.K., Rodríguez-Morgade M.S., Torres T. *Eur. J. Org. Chem*. **2002**, *15*, 2460 – 2464.
23. Krygovski T.M., Cyrański M.K. *J. Chem. Rev*. **2001**, *101*, 1385–1419.
24. Scheyer Pv.R., Maerker C., Dransfeld A., Jiao H., Hommes N.J.Rv.E. *J. Am. Chem. Soc.* **1996**, *118*, 6317-6318.
25. Cyranski M.K., Krygovski T.M., Wiciorowski M., Hommes N.J.Rv.E., Shleyer Pv.R. *Angew. Chem. Int. Ed*. **1998**, *37*, 177-180.
26. Islyaikin M.K., Ferro V.R., García de la Vega J.M. *J. Chem. Soc., Perkin Trans.* 2. **2002**, *12*, 2104 – 2109.
27. Marinina L.E., Mikhalenko S.A., Lukyanets E.A. *Zh. Org. Khim.* **1973**, *43*, 2025-2029. (Russ).
28. Alonso J.M., Martin M.R., De Mendoza J., Torres T., Elguero J. *Heterocycles* **1987**, *26*, 989-1000.

Received 15.04.2008
Accepted 06.06.2008